scientific reports

Check for updates

OPEN

Effects of the Hubbard potential on the NMR shielding and optoelectronic properties of $BiMnVO_5$ compound

H. A. Rahnamaye Aliabad[1]✉, Muhammad Aamir Iqbal[2]✉, F. Amiri-Shookoh[3], Nadia Anwar[4], Sunila Bakhsh[5] & Iván D. Arellano-Ramírez[6]

This study explores the nuclear magnetic shielding, chemical shifts, and the optoelectronic properties of the $BiMnVO_5$ compound using the full-potential linearized augmented plane wave method within the generalized gradient approximation by employing the Hubbard model (GGA + U). The ^{209}Bi and ^{51}V chemical shifts and bandgap values of the $BiMnVO_5$ compound in a triclinic crystal structure are found to be directly related to Hubbard potential. The relationship between the isotropic nuclear magnetic shielding σ_{iso} and chemical shift δ_{iso} is obtained with a slope of 1.0231 and − 0.00188 for ^{209}Bi and ^{51}V atoms, respectively. It is also observed that the bandgap, isotropic nuclear magnetic shielding, and chemical shifts increase with the change in Hubbard potentials (U) of 3, 4, 5, 6, and 7.

The $BiMXO_5$ family is an analogue of the paganoite mineral $BiNiAsO_5$, which was discovered in a quartz matrix (M = Cd, Ca, Mg, Mn, Pb, Ni, and X = V, As, and P). For instance, at high temperatures, $BiPbXO_5$ (X = V, P) exhibits a phase change from a triclinic to a monoclinic crystal system as a result of a significant re-orientation of XO_4. For the solid solutions $BiNi_xCo_{1-x}PO_5$ and $BiCoAsO_5$, transition metals also play a significant role in the complex antiferromagnetic ordering. Both $BiMgVO_5$ and $BiCaVO_5$ were discovered to show photoluminescence properties at room temperature in terms of their optical characteristics. Despite the fact that both $VO4^{-3}$ and Bi^{3+} emitters have similar properties (wide emission and excitation bands associated with a large Stokes shift)[1]. The potential of Bi(III)-containing oxides as oxygen ion conductors, neon yellow pigments, catalysts, ferroelectric, ferro-elastic, and superconducting materials has been investigated, and it is reported that adding divalent or pentavalent cations in addition to Bi has the potential to increase the number of oxides that contain Bi(III). This resulted in the identification of several new compounds, including $BiSr_2V_3O_{11}$, $BiCa_4V_3O_{23}$, $BiBa_2V_3O_{11}$, $BiBa_2V_2PO_{11}$, $BiMg_2AsO_6$, $BiCa_2VO_6$, $BiCd_2VO_6$, $BiCdVO_5$, $Bi_3Ca_9V_{11}O_{41}$, $Bi_2CaV_2O_9$, $Bi_{1-2x}A_{2x}VO_{4-x}$, $BiMg_2VO_6$, and all these compounds were made in an atmosphere of air. Some of these novel compounds showed remarkable characteristics such as nonlinear optical response, ferroelectricity and high oxygen ion conductivity[1,2]. All Mn (II) oxides were reported to be produced in the $BiMnVO_5$ under vacuum or inert-gas conditions. These compounds have a number of interesting characteristics, including selective oxidation, ferroelectricity, catalysis, and vivid yellow pigments due to the presence of the stereo-active Bi^{3+} ion. Despite the synthesis of several compounds containing the magnetic M^{2+} ion, only a small amount of research has been focused on the magnetic characterization of these materials. Due to their unusual (zigzag) spin ladder architecture, the phases $BiM_2V(_P)O_6$ (M = Cu, Mn) have drawn significant attention in terms of their magnetic properties[2,3]. Low-temperature co-fired ceramics such as $BiMVO_5$ (M = Ca, Mg) compounds have attracted considerable attention because of their potential applications in microwave dielectric ceramics, ferroelectric devices, and nonlinear optoelectronics[4]. Magnetic exchange interactions of $BiMPO_5$ (M = Co, Ni) compounds, on the other hand, have been observed within ferromagnetic pairs of metal ions and antiferromagnetic chains[5,6]. Isotropic exchange interactions can also be found in $MFePO_5$ (M = Fe, Co, Ni, Cu)[7,8] and Li-rechargeable batteries made of Li_3Fe_2, $(PO_4)_3$[9].

[1]Department of Physics, Hakim Sabzevari University, Sabzevar, Iran. [2]School of Materials Science and Engineering, Zhejiang University, Hangzhou 310027, China. [3]Faculty of Physics and Nuclear Engineering, Shahrood University of Technology, P. O. Box 3619995161, Shahrood, Iran. [4]School of Materials Science and Engineering, Tsinghua University, Shaw Technical Science Building, Haidian District, Beijing 100084, China. [5]Department of Physics, Balochistan University of Information Technology, Engineering and Management Sciences, Quetta 87300, Pakistan. [6]Department of Physics, Universidad Tecnológica de Pereira, 660003 Pereira, Colombia. ✉email: rahnama@hsu.ac.ir; aamir.hum@gmail.com

For the first time, Xun et al. investigated the iso-structural compound $BiMnVO_5$, using single-crystal X-ray diffraction data to determine its structural details, and reported the parameters as a = 6.912 A°, b = 6.991 A°, c = 5.354 A°, α = 108.55°, β = 95.98°, and γ = 109.73°[3]. These structures were based on MO_4 tetrahedral with M = V, Bi_2O_8 groups, and MnO_6 octahedral sharing one edge to create Mn_2O_{10} groups. The monoclinic symmetry $BiMnPO_5$ structure contains the same components. However, owing to the substantial differences in the connection of the moieties, the triclinic structure for $BiMnVO_5$ cannot be viewed as a distorted variation of the monoclinic $BiMnPO_5$ structure. The magnetic characterization of $BiMnVO_5$ was carried out using measurements of isothermal magnetization, dc-ac magnetic susceptibility, and heat capacity. These findings show that below a transition temperature of 11.5 K, the material changes phases and becomes anti-ferromagnetic. A robust interplay of intra-dimer and inter-dimer (both intra-chain and inter-chain) contacts has been used to explain the long-range antiferromagnetic ordering. With an increase in magnetic field, inconsistency in heat capacity corresponds to the AFM transition to lower temperatures[2,3].

The measurement of magnetic susceptibility, magnetization, and heat capacity has been reported in order to characterize the bulk magnetic properties of the dimeric chain material $BiMnVO_5$[3]. This discovery offers strong support for an antiferromagnetic transition occurring at a transition temperature of around 11.5 K. Additionally, under zero field, the magnetic entropy change reaches a saturation point at 14.6 J mol^{-1} K^{-1}, which is nearly equal to the entire spin entropy of Mn^{2+}. Strong intra-chain and inter-chain contacts between dimers, in addition to intra-dimer interaction, are at play as long-range magnetic order develops in this chain material. Data on heat capacity at low temperatures ($T < T_N$) shows that there is a gap in the spin excitations ($\Delta/kB \approx 5$ K). Additionally, a spin-flop transition is likely due to an abnormality in the slope of the isothermal magnetization below T_N between 30 and 40 K. This material's weak magnetic anisotropy may be the cause of low-field spin-flop transitions and gapped spin wave excitations[3]. By combining information from measurements of isothermal magnetization and in-field heat capacity, one can create a phase diagram in the magnetic field-temperature plane.

$BiMnVO_5$ is a direct bandgap semiconductor with a gap energy of 1.8 eV, and analysis of the density of states demonstrates that transitions from Mn_{3d}/O_{2p} to V_{3d} are responsible for the optical absorption band. According to its photocatalytic performance, $BiMnVO_5$ has the highest level of catalytic activity. When Methylene Blue (MB) has been exposed to visible light for 4 h, almost 98% of it degrades, from which it is established that the primary active components in the photocatalytic process are hydroxyl radicals and photo-generated holes. It can still degrade 85% of MB in 4 h when exposed to visible light after 5 cycles, and its morphology and structure are unaltered, proving that $BiMnVO_5$ is a reliable photocatalyst[3]. Among the various methods, the solid-state nuclear magnetic resonance (SSNMR) technique is used for the study of structural characterization and detailed information on the interactions[10–13]. Density functional theory (DFT) calculations can be extremely powerful for the determination of nuclear magnetic resonance (NMR) spectra[14]. The chemical shifts can be computed in the plane-wave pseudopotential framework to investigate the attributes of a large range of systems[15]. The analysis of chemical shifts has been researched for several decades and has been carried out using a wide range of computational approaches[16–20]. Most NMR experiments take place in the solid or liquid state[21].

The work is aimed at exploring the Hubbard potential (GGA + U) effects on nuclear magnetic shielding, chemical shift and optoelectronic properties of the $BiMnVO_5$ compound in a triclinic crystal symmetry. The optoelectronic and NMR spectra are evaluated based on band structure, density of states, dielectric function, energy loss function, and an isotropic chemical shift, highlighting the enormous potential of these compounds for use in optoelectronic devices and sensing applications. To the best of our knowledge, this is the first study ever conducted on the $BiMnVO_5$ compound. It analyzes the effects of varying the Hubbard parameter (U) on the NMR and optoelectronic properties and provides an approximate result for experimenters to fabricate devices using this material.

Theoretical detail

In this work, all calculations were performed by solving the Kohn–Sham equations by employing a self-consistent scheme of the full potential linearized augmented plane wave (FP-LAPW) method in the framework of density functional theory (DFT)[22] within the generalized gradient approximation along with the Hubbard potential (GGA + U) by employing the Wien2k computer code[23]. Hubbard's model of electron correlation in narrow energy bands was initially investigated by Hubbard, and he formulated this Hubbard model in 1963[24]. Since then, this method has been applied to study high-temperature superconductivity, quantum magnetism, optoelectronic properties, and charge density waves with high accuracy.

Structural data and the radii of the muffin tin spheres for $BiMnVO_5$ compound that are used in this study as references are taken as a space group $P\bar{1}$ with lattice parameters $a = 6.912$ A^0, $b = 6.991$ A^0, $c = 5.354$ A^0, $\alpha = 108.55^0$, $\beta = 95.98^0$, $\gamma = 109.73$, while R_{MT} (Bi) = 2.48 a.u., R_{MT} (Mn) = 2.16 a.u., R_{MT} (V) = 1.64 a.u. and R_{MT} (O) = 1.49 a.u, respectively. The value of k_{max} is used as 7, which is the cut-off for the plane wave, and R is the smallest muffin-tin radius. The value of G_{max} is taken as 12, which is the value of the largest vector in charge density Fourier expansion at the plane wave cut-off. A cut-off energy of − 6 Ry caused the self-consistent computations to converge at 0.0001 Ry.

Results and discussion

The $BiMnVO_5$ compound crystallizes in the space group $P\bar{1}$ and all atoms are located on Wyckoff positions 2i[25]. The analysis of the NMR study includes the computation of nuclear magnetic shielding, isotropic chemical shift, density of states, and electronic band structure analysis. The optical properties are also deeply investigated to analyze the potential of these materials in optoelectronic devices.

Nuclear magnetic shielding. NMR spectroscopy is an effective method for acquiring crucial information about molecular systems in chemistry and biochemistry. The nuclear magnetic shielding for $BiMnVO_5$ within the GGA + U model has been computed, first familiarized by Anisimov et al.[26] and further established by Dudarev et al.[27]. A Hubbard model is adopted to correct the self-interaction error using the following relationship:

$$E_{tot} = E_{DFT} + \frac{U-J}{2}\sum_{\sigma} n_{m,\sigma} - n_{m,\sigma}^2 \tag{1}$$

where n, m, and σ are the atomic-orbital occupation number, the orbital momentum, and the spin index, respectively. Also, U and J show the on-site Coulomb repulsion and the exchange interaction, respectively. The exchange interaction may be incorporated into the Coulomb term to define the effective Hubbard U as $U_{eff} = U - J$[24,26]. The Hubbard potentials utilized in this work are $U_{eff} = U - J = 3, 4, 5, 6\ and\ 7$. The shielding tensor ($\overline{\sigma}$), can be described by three parameters (σ_{xx}, σ_{yy} and σ_{zz}), from which the isotropic chemical shielding (σ_{iso}), can be obtained as follows[28,29]:

$$\sigma_{iso} = \frac{\sigma_{xx} + \sigma_{yy} + \sigma_{zz}}{3} \tag{2}$$

The three primary components of the shielding tensor (σ_{xx}, σ_{yy} and σ_{zz}) can be defined by the Haeberlen, Mehring, and Spiess convention[30–32]. The principal components are defined in the sequence $|\sigma_{zz} - \sigma_{iso}| \geq |\sigma_{yy} - \sigma_{iso}| \geq |\sigma_{xx} - \sigma_{iso}|$.

The chemical shift values (δ_{iso}) of the magnetic shielding of a reference sample and of an unknown sample can be measured as follows[29]:

$$\delta(ppm) = \frac{\sigma_{ref} - \sigma}{1 - \sigma_{ref}} \times 10^6 \tag{3}$$

where σ_{ref} and σ are the magnetic shielding of the reference and the sample, respectively. In this work, the BiI_3O_9 and $VOCl_3$ compounds are considered as ^{209}Bi and ^{51}V, the reference combination. The tensors of magnetic shielding along the x, y, and z directions are first calculated, and the isotropic shielding values are calculated using Eq. (2). On the other hand, the isotropic chemical shift values are evaluated by the isotropic shielding values of $BiMnVO_5$ in different potentials and references compounds to the formula (Eq. 3). The calculated ^{209}Bi and ^{51}V chemical shielding (σ_{ii}), isotropic chemical shift (δ_{iso}) of both the compounds by using $GGA + U\ (U = 3, 4, 5, 6, 7\ \text{eV})$ are presented in Tables 1 and 2, respectively.

The ^{209}Bi and ^{51}V calculated isotropic nuclear magnetic shielding and the ^{209}Bi and ^{51}V measured isotropic chemical shifts are organized in a straight line by reference compounds of BiI_3O_9 and $VOCl_3$, respectively, and are shown in Fig. 1 by yielding relationships $\sigma_{iso}(Bi) = (1.0231)\delta_{iso}(Bi) + 643884.50$ and $\sigma_{iso}(V) = (-0.00188)\delta_{iso}(Bi) - 1875.35$.

Hubbard potentials (U)	σ_{xx}	σ_{yy}	σ_{zz}	σ_{iso}^{Cal}	δ_{iso}
3	2192.52	2192.52	2817.51	2400.85	− 62,7228
4	2191.35	2191.35	2822.30	2401.67	− 62,7100
5	2189.03	2189.03	2826.60	2401.55	− 62,7119
6	2168.95	2204.92	2832.46	2402.11	− 62,7032
7	2165.08	2213.83	2837.23	2405.38	− 62,6524
BiI_3O_9	6718.74	6465.09	6132.72	6438.85	0

Table 1. The calculated components of the chemical-shielding tensor (σ_{ii}), ^{209}Bi isotropic chemical shift (δ_{iso}) by using GGA + U (U = 3, 4, 5, 6, 7 eV) for $BiMnVO_5$. (All values are in ppm).

Hubbard potentials (U)	σ_{xx}	σ_{yy}	σ_{zz}	σ_{iso}^{Cal}	σ_{iso}^{Thoery}	δ_{iso}
3	− 740.14	− 740.14	− 714.13	− 731.47	–	− 609,632
4	− 711.09	− 707.57	− 689.33	− 702.66	–	− 624,986
5	− 671.86	− 671.86	− 694.15	− 679.29	–	− 637,441
6	− 648.07	− 648.07	− 674.28	− 656.81	–	− 649,422
7	− 620.61	− 620.61	− 649.73	− 630.32	–	− 663,540
VOCl3	− 1646.54	− 1658.13	− 321.41	− 1875.36	− 2267.6[a]	0

Table 2. The calculated components of the chemical-shielding tensor (σ_{ii}), ^{51}V isotropic chemical shift (δ_{iso}) by using GGA + U (U = 3, 4, 5, 6, 7 eV) for $BiMnVO_5$. All values are in ppm. [a][33].

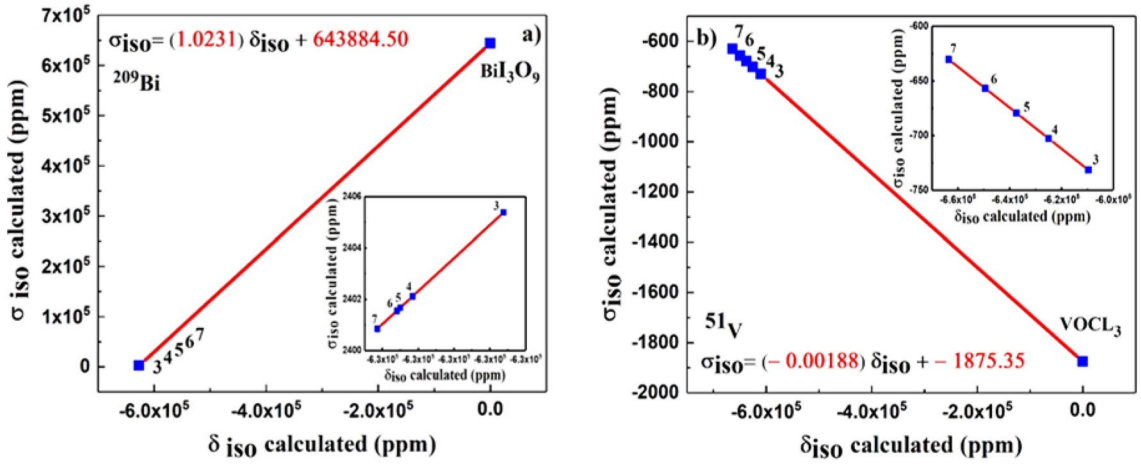

Figure 1. The ^{209}Bi and ^{51}V calculated isotropic nuclear magnetic shielding and the ^{209}Bi and ^{51}V measured isotropic chemical shifts that are organized in a straight line by reference compounds of BiI_3O_9 and $VOCl_3$, (**a**) ^{209}Bi σ_{iso}, and (**b**) ^{51}V σ_{iso}. Insets in both plots show the U-dependance in a deeper detail.

By increasing the U_{eff} parameters, the ^{209}Bi and ^{51}V chemical shielding of the compounds increase from 2400.85 to 2405.38 ppm and from − 731.47 to − 630.32, respectively. As a result, isotropic chemical shift values are also increased. It seems that Hubbard's potential plays an important role in NMR parameters. The obtained results show that the magnetic shielding tensors along the x and y directions are the same ($\sigma_{xx} = \sigma_{yy}$), and these values are less than the tensors along the z-direction (σ_{zz}). Moreover, the calculated ^{209}Bi and ^{51}V chemical shielding and chemical shift are drawn according to Hubbard potential in Fig. 2, and they give $\sigma_{iso}(Bi) = (0.95)U + 2397.562$, $\delta_{iso}(Bi) = (147.6)U - 627738.6$, $\sigma_{iso}(V) = (24.815)U - 804.185$ and $\delta_{iso}(V) = (-13225.2)U - 570878.2$. The obtained results show that calculated ^{209}Bi, ^{51}V σ_{iso} and ^{209}Bi δ_{iso} values increase with increasing Hubbard potential, while ^{51}V δ_{iso} calculated values show a reverse trend with the increase in Hubbard potential. Also, the

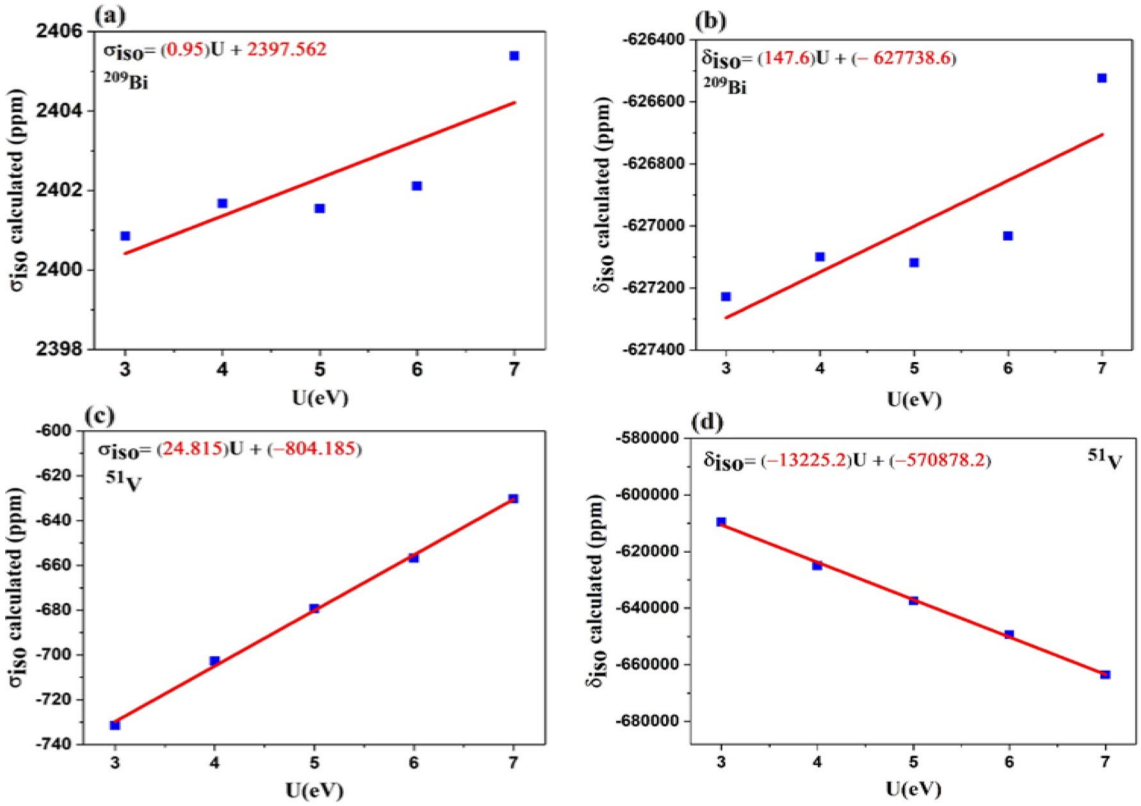

Figure 2. Variation of (**a**) ^{209}Bi σ_{iso} values (ppm), (**b**) ^{209}Bi δ_{iso} values (ppm), (**c**) ^{51}V σ_{iso} values (ppm), and (**d**) ^{51}V δ_{iso} values (ppm), with respect to Hubbard potential.

calculated magnetic shielding for the ^{51}V reference compound, $VOCl_3$, is in close agreement with its theoretical results[33].

The isotropic chemical shielding for Mn and O atoms is also evaluated under the effect of varying Hubbard potential and presented for the $BiMnVO_5$ compound in Table 3. The calculated chemical shielding for Mn atoms increases from 571.95 to 650.47. It can be inferred that there is an indirect link between the calculated chemical shielding for Mn atoms and the static dielectric function. The negative value of isotropic chemical shielding for ^{51}V atoms shows that the external field is strengthened by the electrons.

Electronic properties. In order to deeply analyze the electronic properties, the calculated band structure and density of states within the GGA + U potential with a varying value of U from 3 to 7 for the $BiMnVO_5$ compound are plotted. The distance between the maximum of the valence band and the minimum of the conduction band is usually indicated as the bandgap energy (E_g), and from Fig. 3, it can be easily deduced that bandgap values are of the indirect gap nature as the k-space vector position is located at R-Γ. The energy levels are described by the quantum mechanical formalism in the band structures, and from the band structures of the $BiMnVO_5$ compound, it can be inferred that the targeted material is of semiconductor nature; hence, can be potentially employed in photocatalytic applications. The generated band structures for the $BiMnVO_5$ compound adopting GGA + U ($U = 3, 4, 5, 6$ *and* 7) along with the reference compounds are portrayed in Fig. 3, and bandgap values for the reference compounds are summarized in Table 4.

Hubbard potentials (U)	$\sigma_{iso}(Mn)$	$\sigma_{iso}(O_1)$	$\sigma_{iso}(O_2)$
3	571.95	− 112.76	− 124.19
4	600.38	− 109.39	− 120.87
5	621.10	− 106.53	− 117.11
6	637.31	− 102.02	− 113.40
7	650.47	− 98.72	− 107.90

Table 3. The isotropic chemical shift (σ_{iso}) for Mn and O atoms by using GGA + U (U = 3, 4, 5, 6, 7 eV) for $BiMnVO_5$. All values are in ppm.

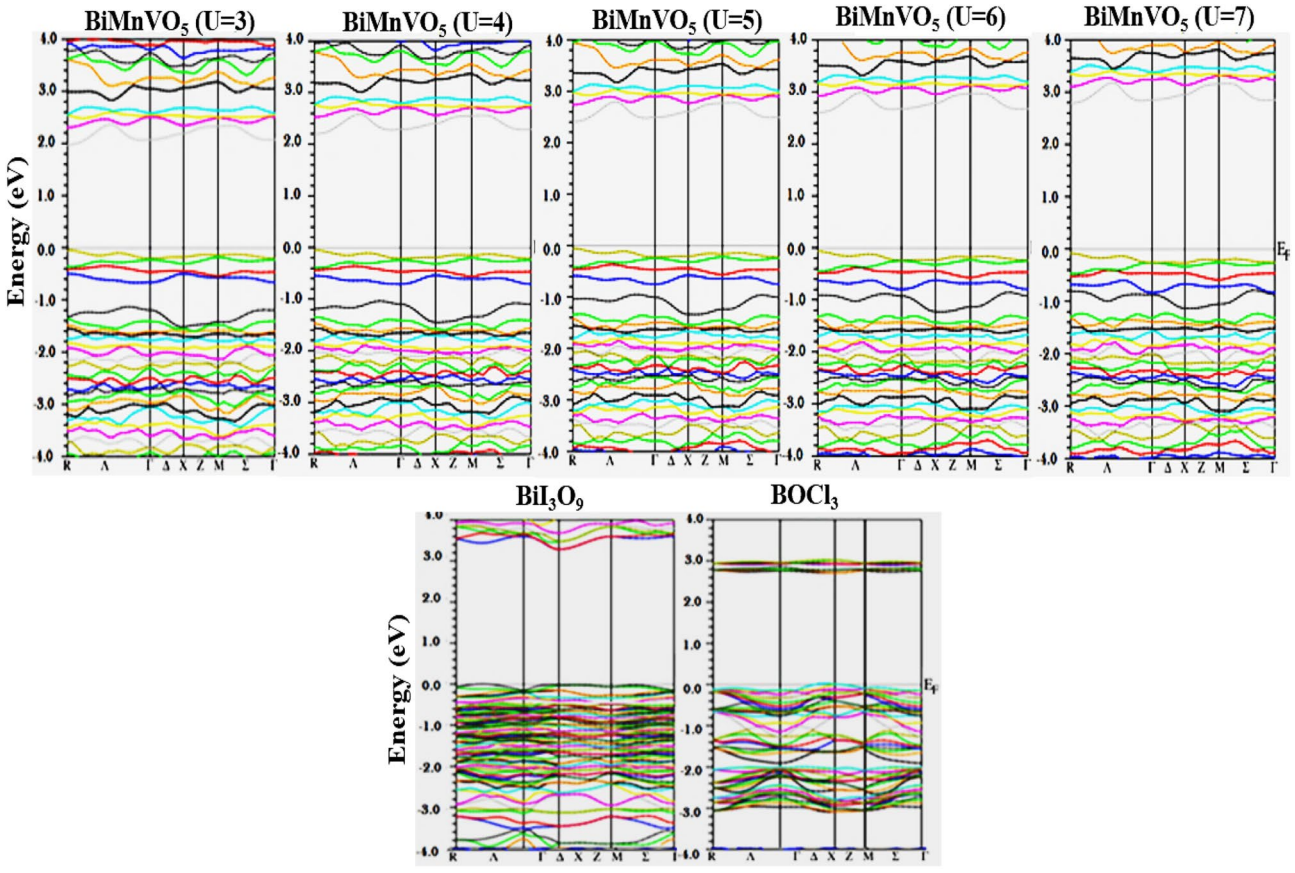

Figure 3. Computed band structures of $BiMnVO_5$ (at U = 3, 4, 5, 6, and 7) along with the reference compounds.

Compounds	Space group	$a_{Exp.}$	$b_{Exp.}$	$c_{Exp.}$	E_g^{GGA}	E_g^{Exp}
BiI_3O_9	$P2_1/n^a$	8.888[a]	5.944[a]	11.221[a]	3.1	2.9[a]
$VOCl_3$	$P2_1/n^b$	4.963[b]	9.140[b]	11.221[b]	2.6	2.8[c]

Table 4. Structural parameters and calculated bandgap values within GGA for references compounds. Lattice parameters and bandgap energy is in (Å) and (eV), respectively. [a34]; [b35]; [c36].

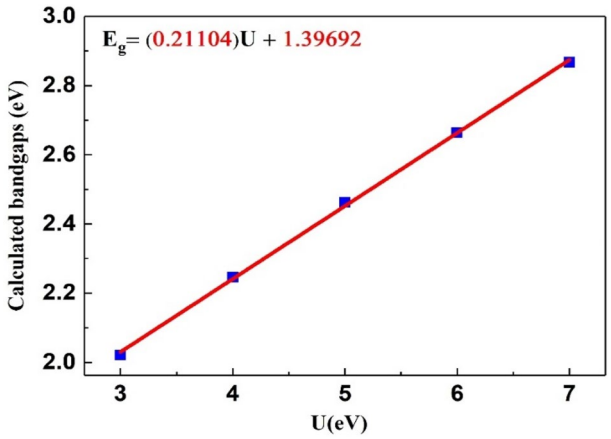

Figure 4. Comparison of calculated bandgap values with respect to Hubbard potential.

The calculated bandgap values are drawn according to Hubbard potential as shown in Fig. 4, and they give the band energy relation as: $E_g = (0.21104)U + 1.39692$. The obtained results show that the bandgap increases with increasing Hubbard potential, from a value of 3–7. It can also be observed that there is an inverse relationship between the bandgap values and the variation in the calculated isotropic chemical shift (δ_{iso}) for the ^{51}V atom. The rise in bandgap may be due to the new electronic potentials generated by utilizing different U parameter values from 3 to 7. These potentials also result in a shift of conduction band electrons by lengthening the distance between the top of the valence band and the lowest of the conduction band.

The density of states (DOS) of a system can be described by the number of states per interval of energy at each energy level that are accessible to be busied by electrons and can be used to represent an in-depth understanding of the electronic attributes of the system. For a system, a high DOS at a specific energy level means that there are many states available for occupation, and a zero DOS means that no states can be occupied at that energy level[37]. The calculated densities of states for the ^{209}Bi, ^{51}V, and Mn atoms are shown in the incident energy range of − 25.0 to 15.0 eV using Hubbard values of U = 3, 4, 5, 6, and 7, as portrayed in Figs. 5, 6, and 7, respectively. The $BiMnVO_5$ compound has the same behavior of DOS at all potentials. For both spin-up and spin-down states, the portion of the valence band at − 25 eV is formed of the Bi-5*d* state except for U = 6 and 7.

From Fig. 5, it can be observed that in the valence band, the Bi-6*s* state exists, whereas the conduction band is composed of the Bi-5*p* state for both spin-up and spin-down states, and these states have an important role in ^{209}Bi magnetic shielding. The density of states peaks at 2.5–5.5 eV in the conduction band, generally owing to the contribution of the Bi-5*p* state. As shown in Fig. 6, for the spin-up state, the portion of the valence band at − 25 eV is primarily composed of the V-4*s* state within GGA + U at U = 5 eV. For the spin-up state, the involvement of the V-3*d* state in the valence band at 0.0–6 eV for a 5 eV potential is greater than that of other potentials. On the other hand, for the spin-up state, the top of the conduction band at 2.5–65 e is mainly influenced by the V-3*d* state in all potentials except for U = 5 eV.

The Mn atom has a considerable role in the calculation of magnetic shielding data. Therefore, the PDOS of Mn-s, Mn-p, and Mn-d states for the $BiMnVO_5$ compound is perused by GGA + U ($U = 3, 4, 5, 6$ *and* 7) as portrayed in Fig. 7. For the spin-up state, the valence band at − 5.0 to 0.0 eV is primarily composed of the Mn-3*d* state, whereas for the spin-down state, these states are located at 2–7 in the conduction band. On the other hand, by moving the value of U from 3 to 7 eV, the intensity of Mn-3*d* peaks in the valence and conduction bands starts to decrease. In the spin-down state, the intensity of Mn-3*d* peaks in the conduction band is very high, and by increasing U_{eff} parameters, the intensity of these peaks decreases. We found that the Mn-3*d*, Bi-*p*, Bi-*d*, and V-3*d* states have a dominating effect on the isotropic magnetic shielding value of the $BiMnVO_5$ compound.

Optical properties. For the calculation of the optical spectra, following relations are used[38,39]:

$$\varepsilon_1(\omega) = \delta_{\alpha\beta} + \frac{2}{\pi} P \int_0^{\infty} \frac{\omega' \mathrm{Im}\varepsilon_{\alpha\beta}(\omega')}{(\omega')^2 - \omega^2} d\omega' \tag{4}$$

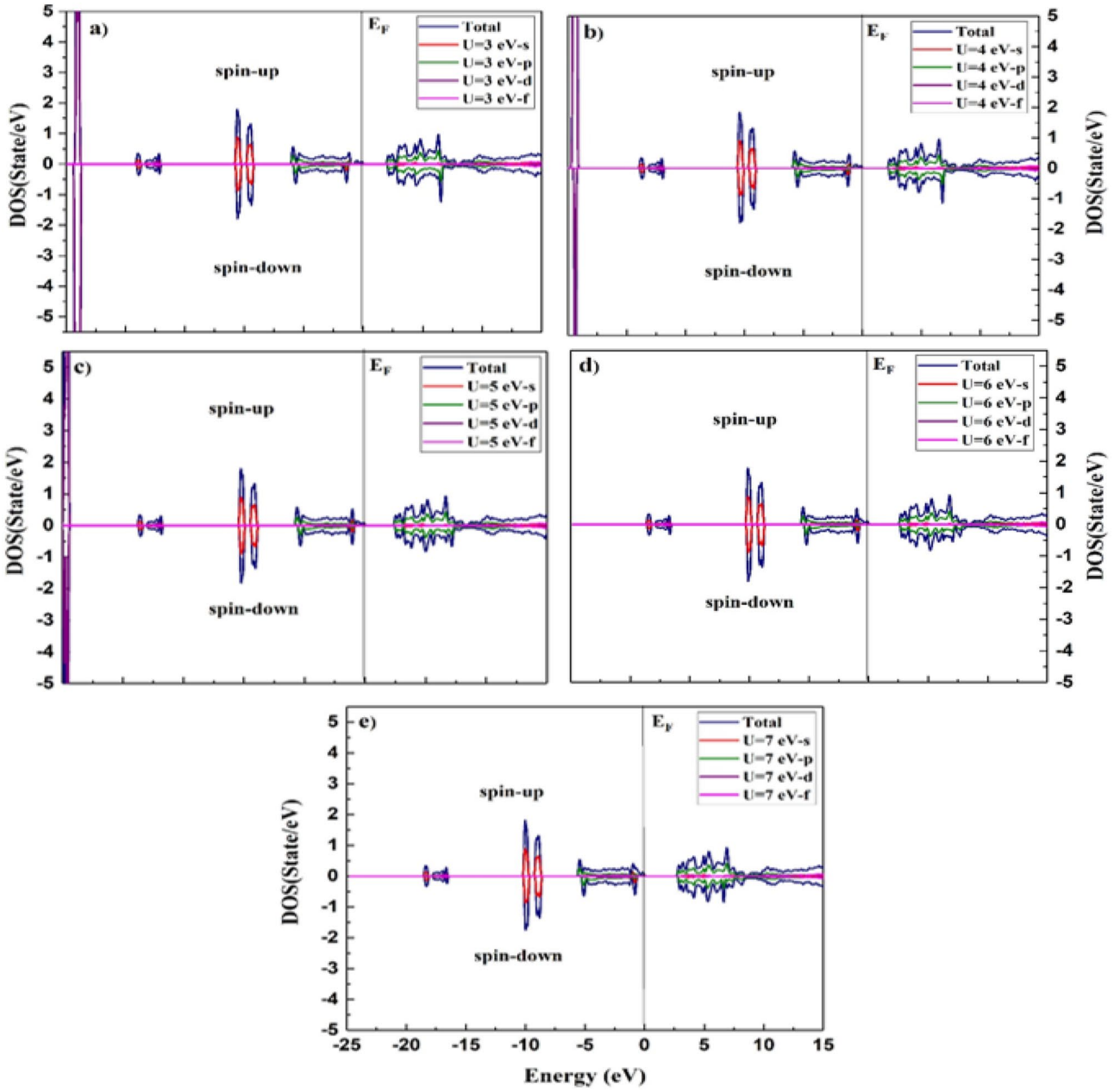

Figure 5. Calculated density of states of $BiMnVO_5$ compound at U = 3, 4, 5, 6, and 7 for ^{209}Bi by using GGA + U scheme.

$$\varepsilon_2(\omega) = \frac{\hbar^2 e^2}{\pi m^2 \omega^2} \sum_{c,v} \int d\mathbf{k} \langle c_k | p^\alpha | v_k \rangle \langle v_k | p^\beta | c_k \rangle \times \delta(\varepsilon_{ck} - \varepsilon_{vk} - \omega) \tag{5}$$

$$L(\omega) = -Im\left[\frac{1}{\varepsilon(\omega)}\right] = \frac{\varepsilon_2(\omega)}{\varepsilon_1^2(\omega) + \varepsilon_2^2(\omega)} \tag{6}$$

$$\hbar\omega_p^e = \hbar\sqrt{\frac{ne^2}{\varepsilon_0 m}} \tag{7}$$

The real, $\varepsilon_1(\omega)$ and imaginary part, $\varepsilon_2(\omega)$ of the dielectric function are shown for the $BiMnVO_5$ compound in the x, y, and z directions. From Fig. 8, it is concluded that by increasing the U_{eff} parameters, the value of the static dielectric function decreases from 5.46 to 4.97 for the $BiMnVO_5$ compound in the x, y, and z directions. It is clear that there is a direct relationship between the static dielectric function, $\varepsilon_1(0)$, and the isotropic chemical

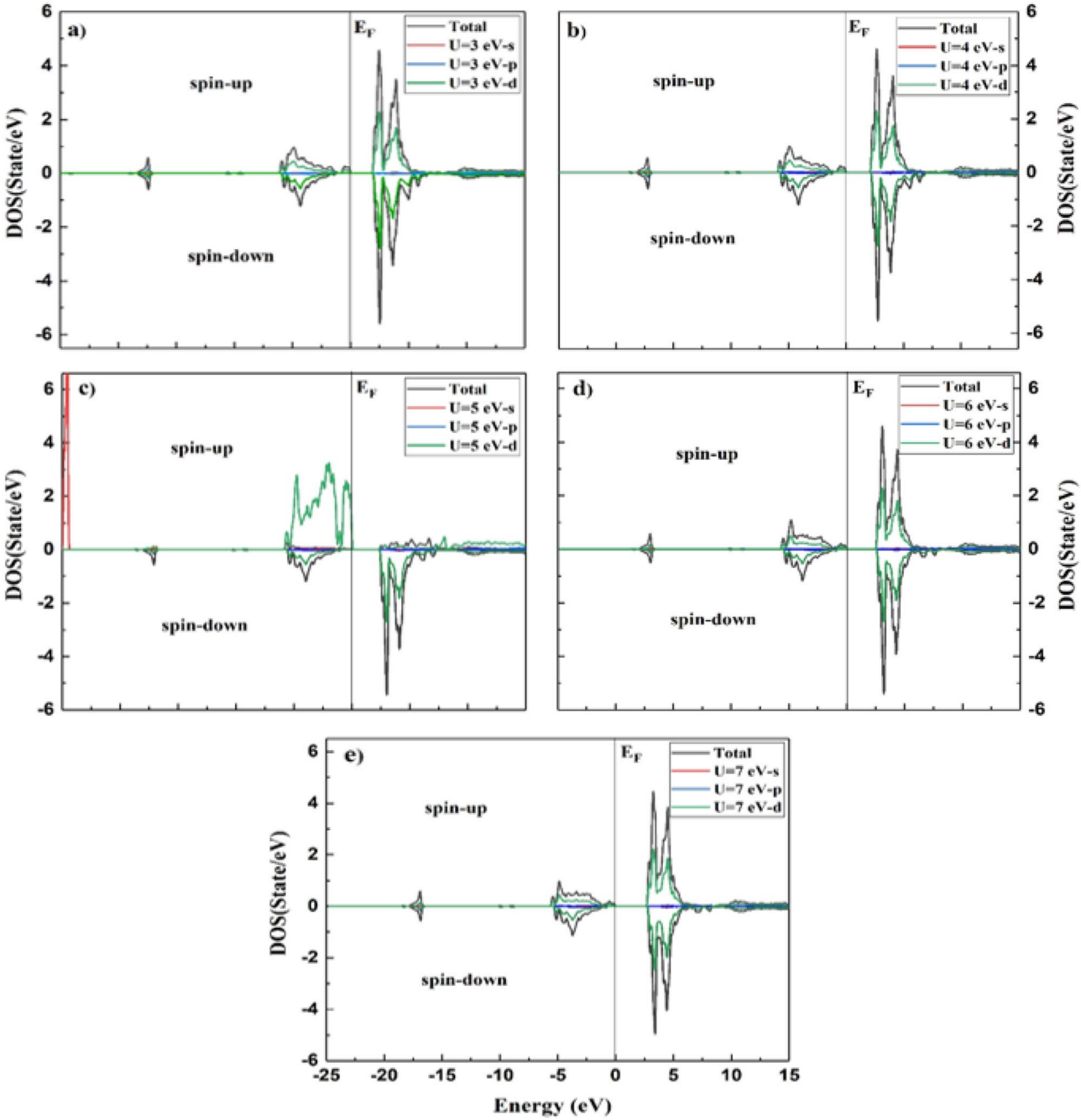

Figure 6. Calculated density of states of $BiMnVO_5$ compound at U = 3, 4, 5, 6, and 7 for ^{51}V by using GGA + U scheme.

shift (δ_{iso}) for the ^{51}V atom. On the other hand, the bandgap increases from 2.0208 to 2.8672, and the obtained results are observed in accordance with the Penn model[40–42].

The maximum peaks of $\varepsilon_1(\omega)$ appear at 35.44, 33.18, and 37.03 for U = 6, 3, and 5 eV in the x, y, and z directions, respectively. As shown in Fig. 8b, the main peak of $\varepsilon_2(\omega)$ is found around 5.82, 4.99, and 6.74 in the x, y, and z directions, respectively. Indeed, these peaks show the transition from the valence band to the conduction band states. With an increase in U from 3 to 7, the main peak value increases, and this behavior confirms the variation in bandgap as well as chemical shielding for Mn atoms.

The variation of refractive index, $n(\omega)$ and extinction coefficient, $k(\omega)$ in the x, y, and z directions is depicted in Fig. 9, from which it can be seen that the spectrum for $n(\omega)$ and $k(\omega)$ pursues the real part $\varepsilon_1(\omega)$ and imaginary part $\varepsilon_2(\omega)$ of the dielectric function, respectively. A small change $k(\omega)$ in $\varepsilon_2(\omega)$ may be due to medium absorption[41], in which incident radiation is absorbed in the material. From Fig. 9a, it is easily depicted that the $n(\omega)$ initially increases and then declines firmly in a small energy interval after reaching the maximum value. Many small peaks are visible in the spectra at intermediate energies, which disappear at higher energies owing to the attraction of high energy photons by $BiMnVO_5$ at different potentials. By increasing U from 3 to 7, the

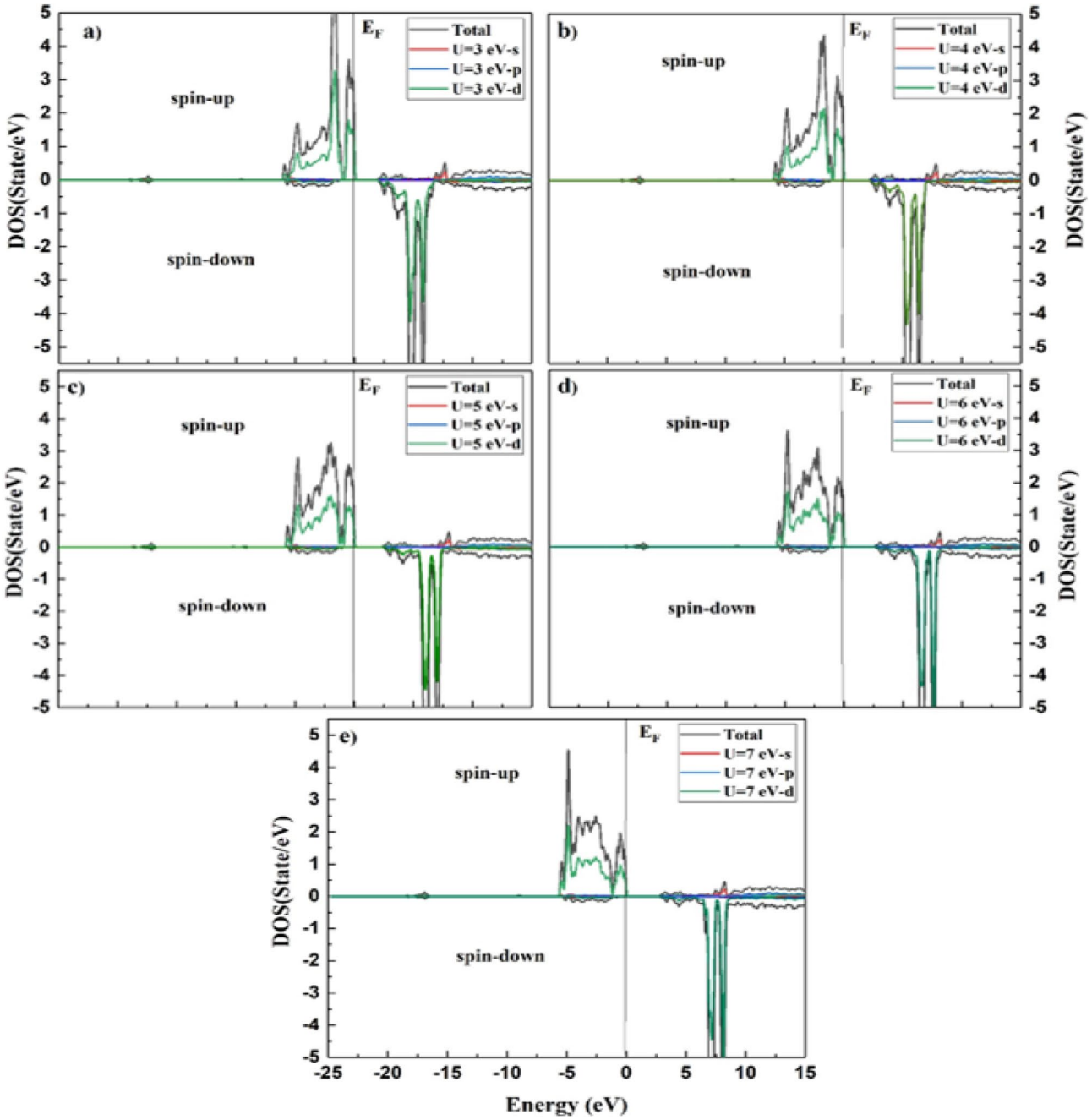

Figure 7. Calculated partial density of states in the spin-up and down states of Mn-s, p and d for $BiMnVO_5$ compound at U = 3, 4, 5, 6, and 7.

value of the static refraction index $n(0)$ decreases in the x, y, and z directions, and this behavior confirms the shift of the isotropic chemical shift (δ_{iso}) for the ^{51}V atom in the $BiMnVO_5$ compound and that it decreases with an increase in Hubbard potential. Insets in all plots of Fig. 9 show the effect of U values in greater detail on the static index of refraction.

The electron energy loss spectrum (EELS) is a useful tool for investigating various material properties[43–45]. The EELS spectrum is plotted in the x, y, and z directions for the $BiMnVO_5$ compound as shown in Fig. 10. The energy of the main maximum and the energy of the volume plasmon are the same. The electron plasmon energy increases by increasing the U_{eff} parameters in the x, y, and z directions, and this treatment is in accordance with a variation in ^{209}Bi and ^{51}V σ_{iso} and ^{209}Bi δ_{iso} calculated values at the Hubbard potential of U = 3, 4,5, 6, and 7. Insets in all plots of Fig. 10 show the effect of U values in greater detail on the energy loss function with an incident energy range of 22–25 eV, from which it can be seen that the electron energy loss increases as the U values increase from 3 to 7, and a maximum loss function has been observed at a high value of the Hubbard parameter.

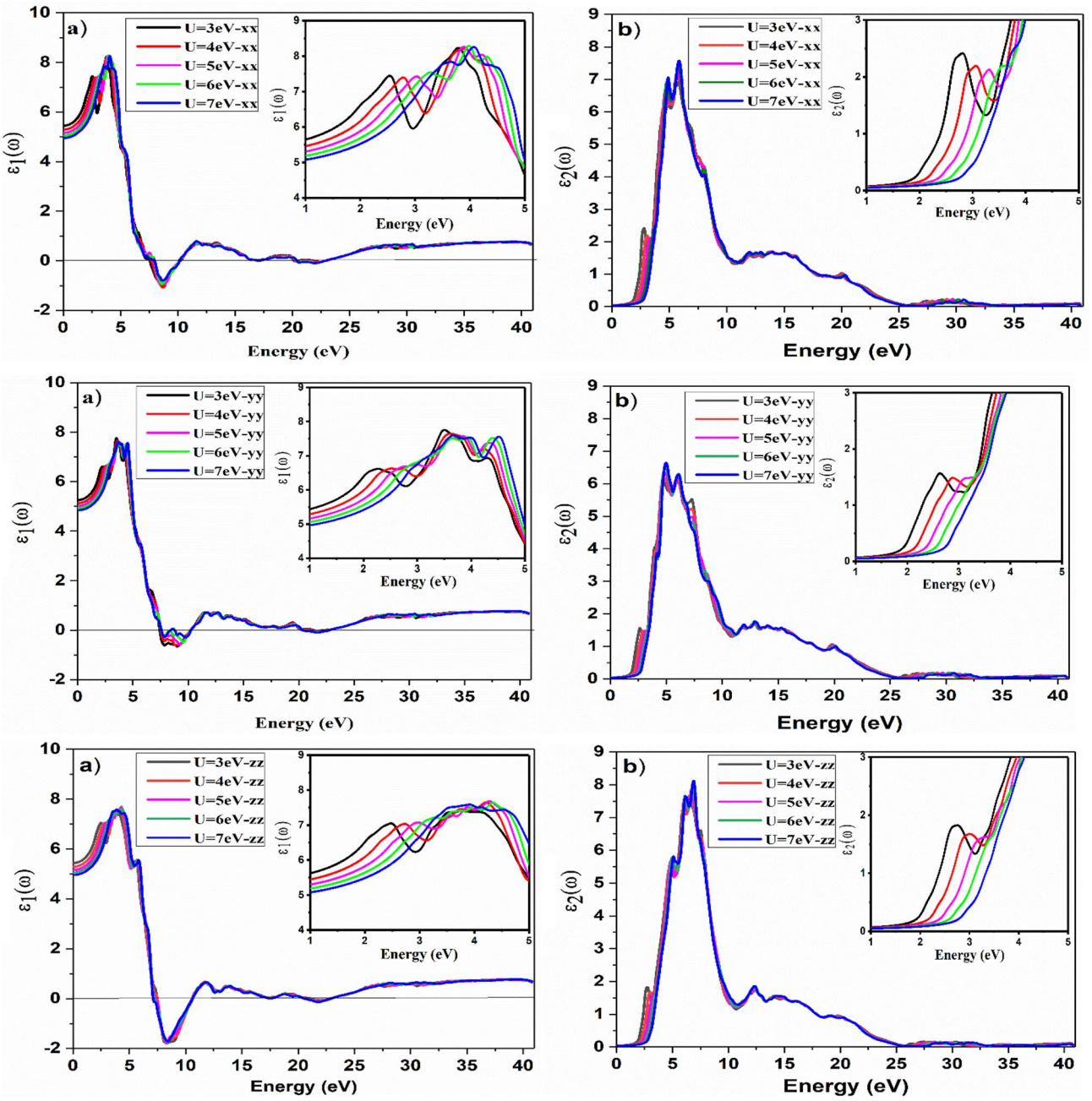

Figure 8. Effect of the Hubbard parameter on the optical spectra for $BiMnVO_5$ compound at U = 3, 4, 5, 6, and 7, for (**a**) the real part of dielectric function and (**b**) the imaginary part of dielectric function, in the x, y, and z directions, respectively. Insets in all plots show the effect of U values in greater detail.

Conclusions

This study reports the ^{209}Bi and ^{51}V magnetic shielding, electronic, and optical properties of the $BiMnVO_5$ compound within the GGA + U approximation by employing DFT. The obtained results show that Hubbard potential changes the shielding values, bandgap, and optical properties. The calculated ^{51}V σ_{iso} and δ_{iso} values show that there is an inverse relationship between the ^{51}V NMR shielding data and bandgap values. On the other hand, it seems that there is a direct relation between the ^{51}V chemical shift and the static dielectric function. The calculated PDOS patterns show that the valence band is mainly composed of the Bi-s state, whereas the conduction band is primarily composed of the Bi-p state for both spin-up and spin-down states, and these states play an important role in ^{209}Bi magnetic shielding. Nevertheless, the Hubbard potential approach is successful in predicting theoretical NMR chemical shifts for ^{209}Bi and ^{51}V nuclei and optoelectronic properties of correlated systems.

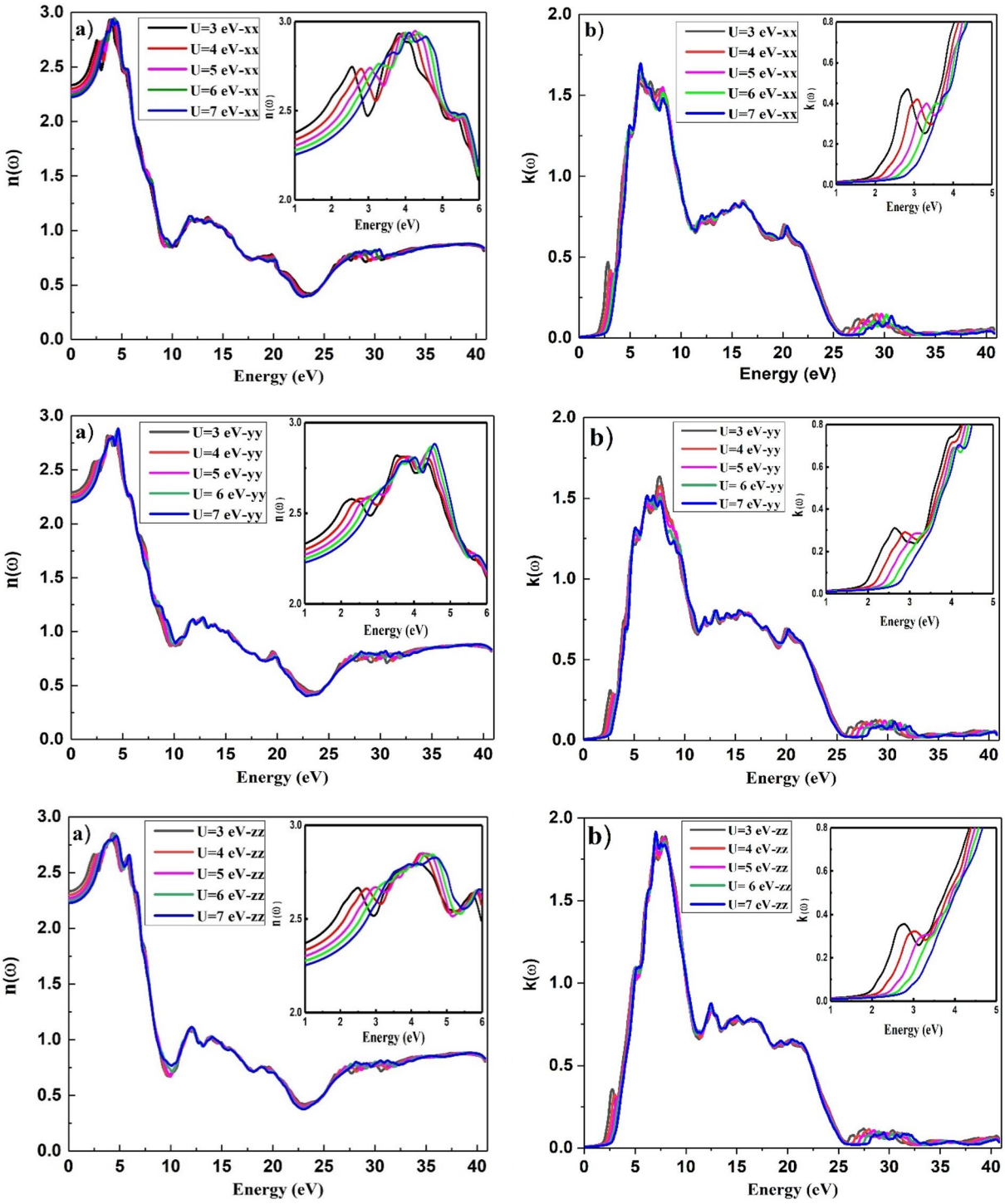

Figure 9. Effect of the Hubbard parameter on the refraction spectra for $BiMnVO_5$ compound at U = 3, 4, 5, 6, and 7 for, (**a**) refractive index and (**b**) extinction coefficient, in the x, y and z directions, respectively. Insets in all plots show the effect of U values in greater detail.

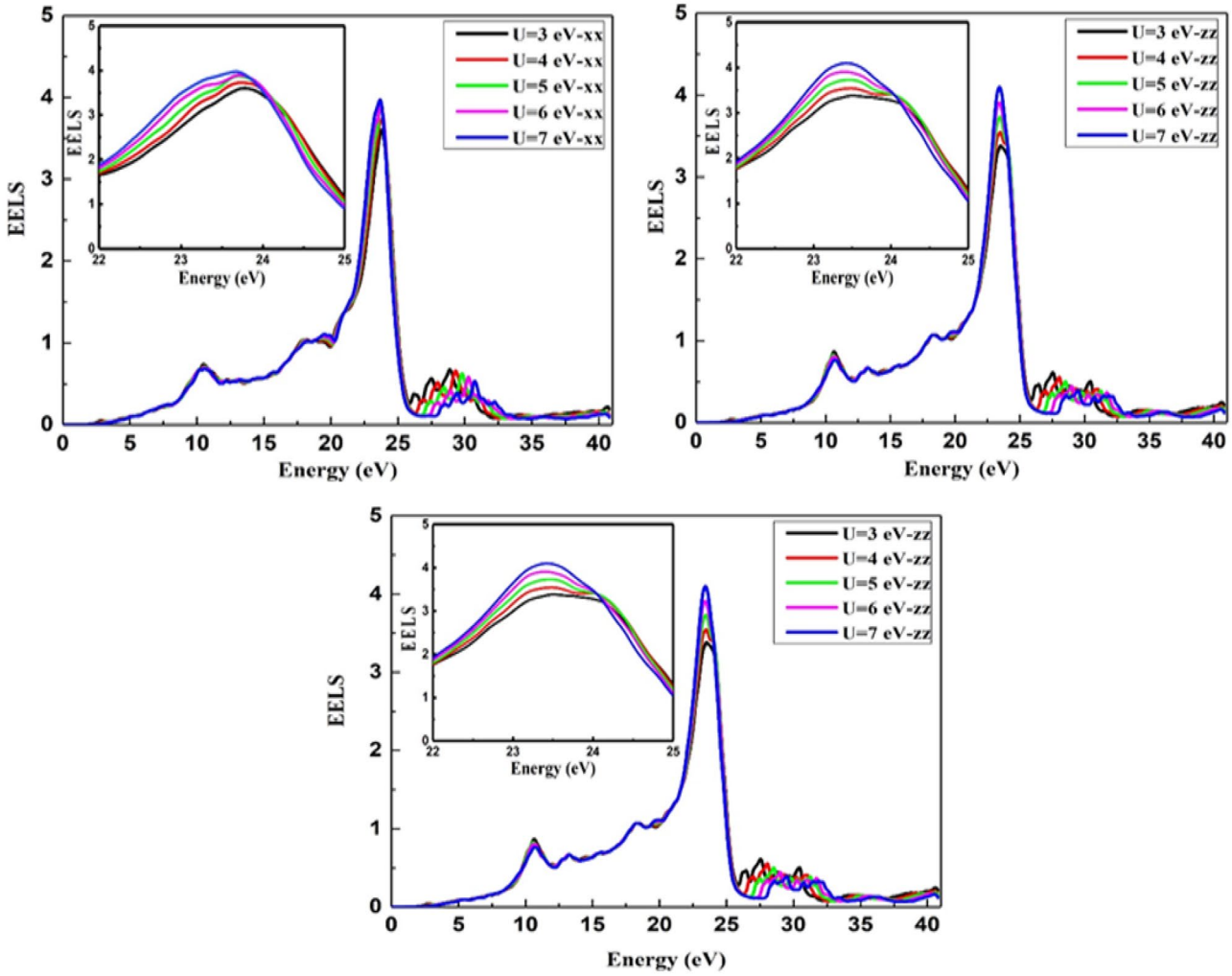

Figure 10. Effect of the Hubbard parameter on the energy loss spectrum for $BiMnVO_5$ compound by GGA + U (U = 3, 4, 5, 6, and 7) in the x, y and z directions, respectively. Insets in all plots show the effect of U values in greater detail.

Data availability

The datasets used and analyzed during the current study are available from the corresponding author (H. A. Rahnamaye Aliabad) on a reasonable request.

Received: 10 October 2022; Accepted: 6 April 2023
Published online: 10 April 2023

References

1. Olchowka, J. *et al.* Bismuth and vanadate activators in $BiMVO_5$ (M= Ca, Mg, Cd) phases: Structural, electronic and optical specificities. *J. Alloys Compd.* **709**, 373–380 (2017).
2. Chowki, S. *et al.* Long-range antiferromagnetic order and possible field induced spin-flop transition in $BiMnVO_5$. *J. Phys.: Condens. Matter* **28**(48), 486002 (2016).
3. Xun, X., Yokochi, A. & Sleight, A. W. Synthesis and structure of BiMnVO5 and $BiMnAsO_5$. *J. Solid State Chem.* **168**(1), 224–228 (2002).
4. Kai, C. *et al.* Phase formation and microwave dielectric properties of Bi MVO_5 (M= Ca, Mg) ceramics potential for low temperature co-fired ceramics application. *J. Am. Ceram. Soc.* **102**(1), 362–371 (2019).
5. Pei, Z., Van Dijken, A., Vink, A. & Blasse, G. Luminescence of calcium bismuth vanadate ($CaBiVO_5$). *J. Alloys Compd.* **204**(1–2), 243–246 (1994).
6. Benmokhtar, S. *et al.* Synthesis, crystal structure and optical properties of BiMgVO5. *J. Solid State Chem.* **177**(11), 4175–4182 (2004).
7. Warner, J. K., Cheetham, A. K., Cox, D. E. & Von Dreele, R. B. Valence contrast between iron sites in alpha-Fe_2PO_5: A comparative study by magnetic neutron and resonant x-ray powder diffraction. *J. Am. Chem. Soc.* **114**(15), 6074–6080 (1992).
8. El Khayati, N. *et al.* Crystal and magnetic structures of the oxyphosphates $MFePO_5$ (M= Fe Co, Ni, Cu): Analysis of the magnetic ground state in terms of superexchange interactions. *Eur. Phys. J. B Condens. Matter Complex Syst.* **22**(4), 429–442 (2001).
9. Rousse, G., Rodríguez-Carvajal, J., Wurm, C. & Masquelier, C. Magnetic structural studies of the two polymorphs of $Li_3Fe_2(PO_4)_3$: Analysis of the magnetic ground state from super-super exchange interactions. *Chem. Mater.* **13**(12), 4527–4536 (2001).
10. Hahn, E. L. Nuclear induction due to free larmor precession. *Phys. Rev.* **77**, 297–299 (1950).

11. Crane, J. H. *Separation of $VOCl_3$ from $TiCl_4$ using soya oil*. PhD diss., UCL (University College London, 2014).
12. Knight, W. D. Electron paramagnetism and nuclear magnetic resonance in metals. *Solid State Phys.* **2**, 93 (1956).
13. Weingarth, M. & Baldus, M. *Introduction to biological solid-state NMR*. 1–17. ISBN 978-1-84973-910-8 (2014).
14. Dell, L. A., Ratcliffe, Ch. I., Kong, X. & Wu, G. Multinuclear solid-state nuclear magnetic resonance and density functional theory characterization of interaction tensors in taurine. *J. Phys. Chem. A* **116**, 1008–1014 (2012).
15. Payne, M. C., Teter, M. P., Allan, D. C., Arias, T. A. & Joannopoulos, J. D. Iterative minimization techniques foe ab initio total-energy calculations: molecular dynamics and conjugate gradients. *Rev. Mod. Phys.* **64**, 1045 (1992).
16. Kaupp, M., Buhl, M. & Malkin, V. G. "Calculations of NMR and EPR of parameters: Theory and applications. *Chem. Phys. Chem.* **6**, 557–559 (2005).
17. Helgaker, T., Jaszunski, M. & Ruud, K. Ab initio methods for the calculation of NMR shielding and indirect spin-spin coupling constants. *Chem. Rev.* **99**(1), 293–352 (1999).
18. Facelli, J. C. Calculations of chemical shieldings: Theory and applications. *J. Wiley Online Libr.* **20**, 42–69 (2004).
19. Varra, J. Theory and computation of nuclear magnetic resonance parameters. *Phys. Chem. Chem.* **9**, 5399 (2007).
20. Casabianca, L. B. & de Dios, A. C. Ab initio calculations of NMR chemical shifts. *J. Chem. Phys.* **128**, 052201 (2008).
21. Bjornsson, R., Fruchtl, H. & Buhl, M. ^{51}V NMR parameters of $VOCl_3$: Static and dynamic density functional study from the gas phase to the bulk. *Phys. Chem. Chem. Phys.* **13**, 619–627 (2011).
22. Iqbal, M. A. *et al.* Fundamentals of Density Functional Theory: Recent Developments, Challenges and Future Horizons. *Density Functional Theory-RecentAdvances, New Perspectives and Applications* (2021).
23. Blaha, P., Schwarz, K., Madsen, G., Kvansnicka, D. & Luitz, J. J. Inst. fur Materials Chemistry (TU Vienna) https://www.wien2k.at/.
24. Hubbard, J. Electron correlations in narrow energy bands. *Proc. R. Soc. Lond. A* **276**, 238–257 (1963).
25. Xun, X. *Synthesis and Structure of New Transition Metal Containing Bismuth oxides* (Oregon State University, 2003).
26. Anisimov, V. I., Zaanen, J. & Anderson, O. K. Band theory and Mott insulators: Hubbard U instead of Stoner I. *Phys. Rev. B.* **44**, 943–954 (1991).
27. Dudarev, S. L., Botton, G. A., Savrasov, S. Y., Humphreys, C. J. & Sutton, A. P. A. Electron-energy-loss spectra and the structural stability of nickel oxide: An Isda+u study. *Phys. Rev. B.* **57**, 1505–1509 (1998).
28. Laskowski, R., Blaha, P. & Tran, F. Assessment of DFT functionals with NMR chemical shifts. *Phys. Rev. B* **87**, 195130–195138 (2013).
29. Saito, H. & Ando, I. Chemical shift tensor-the heart of NMR: insight into biological aspects of proteins. *Prog. Nucl. Mag. Res. Sp.* **75**, 181–228 (2010).
30. Haeberlen, U. High-Resolution NMR in Solids. Selective Averaging. In *Advances inMagnetic Resonance Series, Supplement 1*, (Academic Press, 1976).
31. Mehring, M. *Principles of High Resolution NMR in Solids* 2nd edn. (Springer, 1983).
32. Spiess, H. W. *In NMR, Basic Principles and Progress*, Vol. 15 (eds Diehl, P. et al.) p. 55 (Springer, Berlin, 1978).
33. Bjornson, R., Fruchtl, H. & Buhl, M. ^{51}V NMR parameters of $VOCl_3$: Static and dynamic density functional study from the gas phase to the bulk. *Phys. Chem. Chem. Phys.* **13**, 619–627 (2011).
34. Bentria, B., Benbertal, D., Beucher, M. B., Masse, R. & Mosset, A. Crystal structure of anhydrous bismuth iodate, Bi $(IO_3)_3$. *J. Chem. Crystallogr.* **33**(11), 867–873 (2003).
35. Galy, J., Enjalbert, R. & Jugil, G. $VOCl_3$: Crystallization, crystal structure, and structural relationships: A joint X-ray and 35Cl-NQR investigation. *J. Solid State Chem.* **47**, 143–150 (1983).
36. Diaz, C. *et al.* Crystallizing vanadium pentoxide nanostructures in the solid state using modified block copolymer and chitosan complexes. *J. Nanomater.* **16**, 117–117 (2015).
37. Bououdina, M. (ed.) (IGI Global, 2014).
38. Wooten, F. *Optical Properties of solid* (Academic Press, 1972).
39. Fox, M. *Optical Properties of Solid* (Oxford University Press, 2001).
40. Hosseini, S. M., Rahnamaye Aliabad, H. A. & Kompany, A. First-principles study of the optical properties of pure α-Al_2O_3 and La aluminates. *Eur. Phys. J. B Condens. Matter Complex Syst.* **43**(4), 439–444 (2005).
41. Kittel, C. *Introduction to Solid State Physics* 8th edn. (Wiley, 2005).
42. Iqbal, M. A. *et al.* Ab-initio study of pressure influenced elastic, mechanical and optoelectronic properties of $Cd_{0.25}Zn_{0.75}Se$ alloy for space photovoltaics. *Sci. Rep.* **12**(1), 1–2 (2022).
43. Iqbal, M. A. *et al.* Unveiling concentration effects on the structural and optoelectronic characteristics of Zn1−xCdxS (x= 0,0.25,0.50,0.75,1) cubic semiconductors: A theoretical study. *RSC Adv.* **12**(35), 22783–91 (2022).
44. Iqbal, M. A., Malik, M. & Shahid, W. Theoretical investigations on structural and optoelectronic properties of Bismuth oxyhalides. *Int. J. Mod. Phys. B* **35**(30), 2150303 (2021).
45. Loughin, S., French, R. H., De Noyer, L. K., Ching, W. Y. & Xu, Y. N. Critical point analysis of the interband transition strength of electrons. *J. Phys. D Appl. Phys.* **29**(7), 1740 (1996).

Acknowledgements

The authors are thankful to Prof. Blaha and Prof. Madsen of the Vienna University of Technology, Austria, for their help in the use of Wien2k. The authors also acknowledge the support provided by Zhejiang University, China.

Author contributions

Conceptualization, H.A.R.A., and M.A.I.; Resources, H.A.R.A.; methodology, H.A.R.A., F.A.S., and M.A.I.; writing-original draft preparation, H.A.R.A., M.A.I., and F.A.S.; writing-review and editing, M.A.I., H.A.R.A., N.A., S.B., and I.D.A-R.; validation, H.A.R.A.; project administration, H.A.R.A., and M.A.I.; funding acquisition, H.A.R.A. All authors have read and agreed to the published version of the manuscript.

Competing interests

The authors declare no competing interests.

Additional information

Correspondence and requests for materials should be addressed to H.A.R.A. or M.A.I.

Reprints and permissions information is available at www.nature.com/reprints.

Publisher's note Springer Nature remains neutral with regard to jurisdictional claims in published maps and institutional affiliations.